Communication

Evaluation of a Ground Subsidence Zone in an Urban Area Using Geophysical Methods

Lara De Giorgi , Dora Francesca Barbolla , Chiara Torre , Stefano Settembrini , Giovanni Leucci *

Posted Date: 26 May 2023

doi: 10.20944/preprints202305.1891.v1

Keywords: GPR; ERT; urban area; ground subsidence risk; limestone cavity

Communication

Evaluation of a Ground Subsidence Zone in an Urban Area Using Geophysical Methods

Lara De Giorgi [1], Dora Francesca Barbolla [1], Chiara Torre [2], Stefano Settembrini [3] and Giovanni Leucci [2,*]

[1] institute of Heritage Science, National Research Council; lara.degiorgi@cnr.it, dora.barbolla@ispc.cnr.it, giovanni.leucci@cnr.it
[2] University of Catania; chiara.torre@phd.unict.it
[3] freelance geologist; info@geostudisettembrini.it
* Correspondence giovanni.leucci@cnr.it

Abstract: The sinking of cavities in urban areas is a very important geological risk to which many towns in Puglia are exposed. The study, mapping, geological and speleological description, classification and cataloging of forms and types of cavities is of fundamental importance for each urban center because it is linked to past local anthropic and natural processes, unique to each site. All this could lead to an enhancement of existing underground cavities in urban areas through conservation and continuous monitoring. Unfortunately in many cases these underground cavities have been used as landfills and subsequently abandoned. One of these cavities at the end of March 2007 collapsed in the inhabited center of Gallipoli causing damage to the structures and fortunately not to human lives. In the area relating to the collapsed cavity, a series of geophysical investigations were undertaken with the use of ground penetrating radar methodology in an attempt to delimit the area of collapse and understand the possible types of interventions for restoring the area. In the same area the measures were repeated 16 years later (December 2022) due to another collapse. The results show a much more widespread danger situation.

Keywords: GPR; ERT; urban area; ground subsidence risk; limestone cavity

1. Introduction

Puglia is one of the Italian regions most affected by the subsidence of the soil due to the subsidence and collapse of natural and anthropic cavities [1,2]. Such events sometimes destroy or threaten the integrity of infrastructures, even of a particular importance, such as roads and railway lines [3]. The repetitiveness of the instability phenomena characterises Salento. This high frequency is linked to the area's geology and especially to the evolution of karst processes and human activities of exploitation of subsoil resources and settlement in the area. In particular, the city of Gallipoli is located on the Ionian coast of Salento (Figure 1). The eastern part of the town of Gallipoli was affected from the end of the 1800s to the beginning of the 1900s by intense underground mining activity due to calcarenite deposits. These deposits, having good mechanical properties, were used to produce tuff ashlars and as ornamental stones for external surfaces [2,3].

The discovery depth of the calcarenite deposit varies between 2 m and 25 m. The mining activity developed through large halls with randomly arranged square pillars with sides equal to 2 or 3 m (Figure 2). The deposit was reached through vertical wells commonly called bell-shaped due to their shape. At the end of the exploitation, the quarries were abandoned and often used as waste deposits, and the relative accesses were blocked and buried until they lost consciousness and memory. At the end of March 2007, there was an important collapse event of the roadway (Figure 3) [2,3].

Preprints (www.preprints.org) | NOT PEER-REVIEWED | Posted: 26 May 2023 doi:10.20944/preprints202305.1891.v1

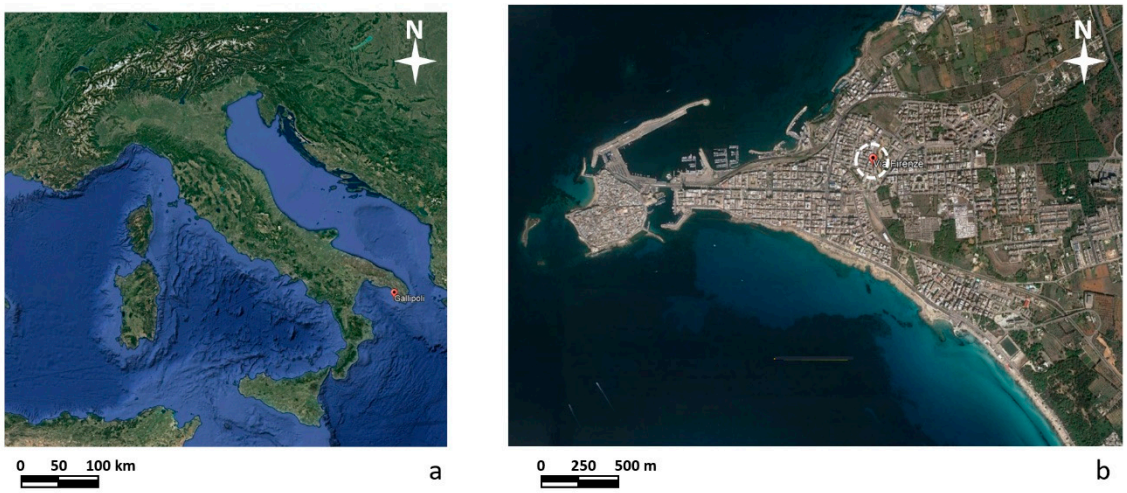

Figure 1. a) map of Italy with the location of Gallipoli, b) map of Gallipoli with the location of the investigated area.

Figure 2. The internal part of the calcarenite quarry.

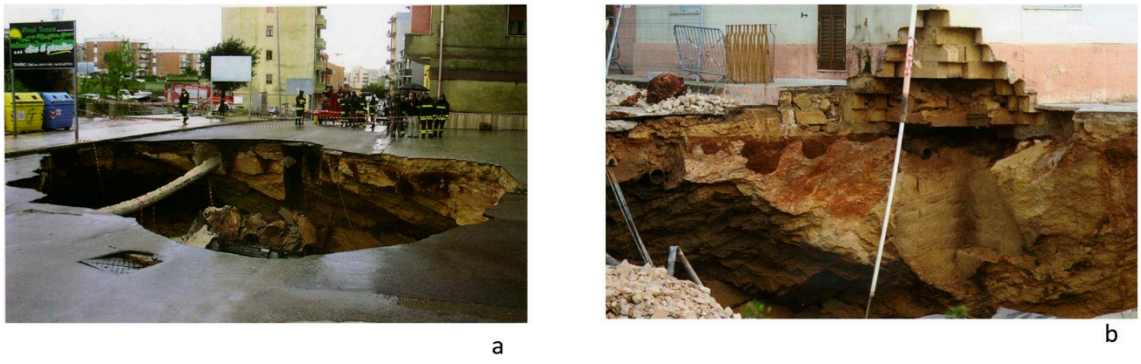

Figure 3. Collapse phenomena occurred at the end of March 2007.

The collapse event had as precursors the deformation of the road surface, also indicated by the slippage of a maintenance hole cover placed on the roadway, which then collapsed a few days before the collapse; the subsidence of the street level indicated by cracks detected on the buildings involved in the instability. The sinking was preceded by days of more or less intense and prolonged rain. The collapse, which saw the formation of a chasm 12 m in diameter and 8 m deep, involving two buildings which housed 16 families, was accompanied by the formation of fractures in the vaults with the detachment of large blocks and suspended boulders. For this reason, geophysical investigations were

 doi:10.20944/preprints202305.1891.v1

necessary for the area affected by the collapse to identify any other danger zones and to identify safe routes for the transit of mechanical means to carry out the work to make the unsafe buildings safe and prevent new collapses. Given the urgency of this first intervention, it was decided to use the ground penetrating radar (GPR) methodology.

Twenty-two years after the instability phenomenon in the same area, in December 2022, there was a slight sinking of the road pavement (Figure 4). For this reason, further geophysical investigations were necessary to verify the extent of the phenomenon. In this case, electrical resistivity tomography (ERT) and GPR were used.

Figure 4. Collapse phenomena occurred at the end of December 2022.

International scientific literature reports many applications of geophysics in areas at risk of subsidence [4–14]. The risk was often linked to natural cavities formed over the years in karst environments. In the case of this paper, the cavities are known because they are cavities dug by man and abandoned. These cavities, over the years, have become a problem for safety.

The geophysical investigation in the case study made it possible to outline the areas not at risk, facilitating the restoration and safety measures. Fifteen years after the first instability event, the geophysical investigations show that the risk is still present and that the consolidation interventions carried out in 2007 must be redesigned.

2. Materials and Methods

For the first geophysical surveys, those of 2007, the georadar of Mala geoscience with a 250 MHz antenna was used. GPR measurements were performed in areas A, B, C, D and E (Figure 5).

Preprints (www.preprints.org) | NOT PEER-REVIEWED | Posted: 26 May 2023 doi:10.20944/preprints202305.1891.v1

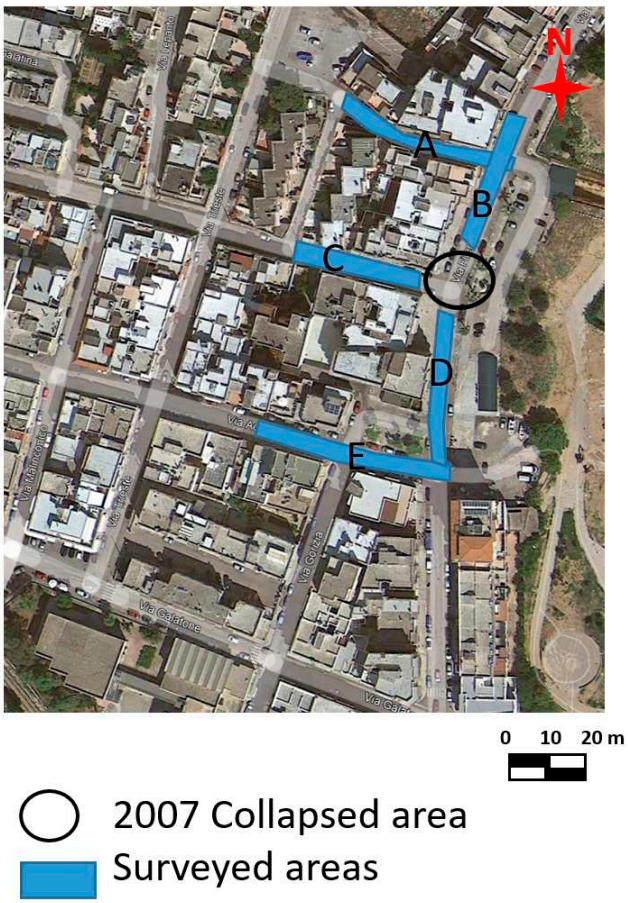

Figure 5. GPR surveyed areas in 2007.

GPR data were acquired in a grid with parallel profiles spaced 0.5 m.

The two-way time window was 100 ns (nanoseconds). The sample interval and the trace interval were, respectively, 512 samples per scan and 0.02m. GPR data were processed using GPR-Slice Software (GPR-SLICE Software (gpr-survey.com)). The 2D data have been processed as the following processing steps: (i) bandpass filter to eliminate both low and high-frequency noise components; (ii) manual adjustment of the gain to try to improve the vision of the deepest reflection events; (iii) background removal filter to eliminate the horizontal components of the signal present on the radar sections and due to ringing; (iv) Kirchhoff migration using an average velocity value of the electromagnetic wave equal to 0.108 m/ns. Electromagnetic (EM) wave velocity can be estimated from GPR data in several ways; the conventional method involves common depth-point (CDP) and wide-angle reflection and refraction (WARR) data sets. Both methods require two antennas in separate units and relatively long acquisition times [9,10]. The EM wave velocity can be more quickly and easily determined from the reflection profiles acquired in continuous mode, using the characteristic hyperbolic shape of reflection from a point source (diffraction hyperbola) [9–12]. This is a very common method for the EM velocity estimation and based on the phenomenon that a small object (the dimensions of the object are smaller than the wavelength of the EM wave introduced in the ground), reflects EM waves in almost every direction. Figure 6 shows an example of application of the above described method applied to the data acquired in the investigated areas.

Preprints (www.preprints.org) | NOT PEER-REVIEWED | Posted: 26 May 2023 doi:10.20944/preprints202305.1891.v1

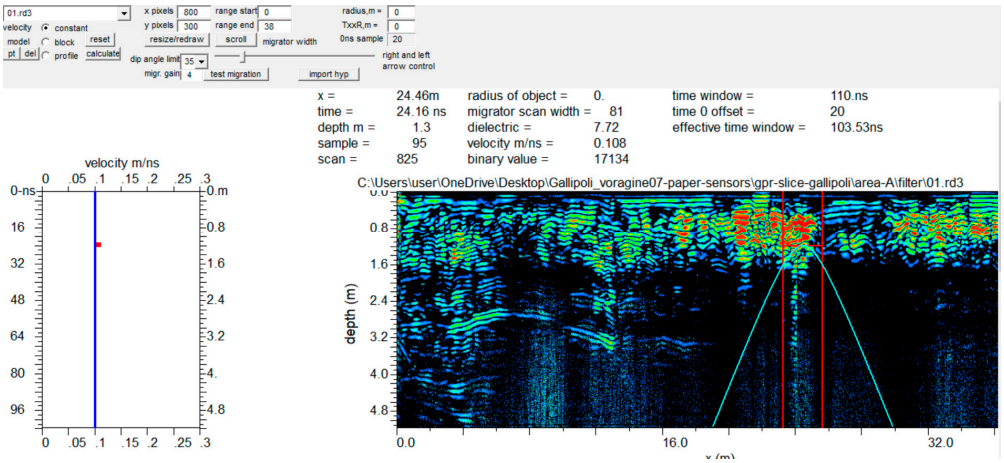

Figure 6. EM wave velocity analysis on 2D radar section. The esteemed EM velocity was 0.108 m/ns.

The data thus processed were subsequently used for constructed 3D volumes. This allows viewing the data in various ways and subsequently simplifying their interpretation.

For the second geophysical survey of 2022, the georadar Ris Hi-mod with a dual-band antenna of 200-600 MHz was used. The location of GPR profiles is shown in Figure 7. Also, in this case, GPR data were processed using GPR-Slice Software (GPR-SLICE Software (gpr-survey.com)) with the same processing steps.

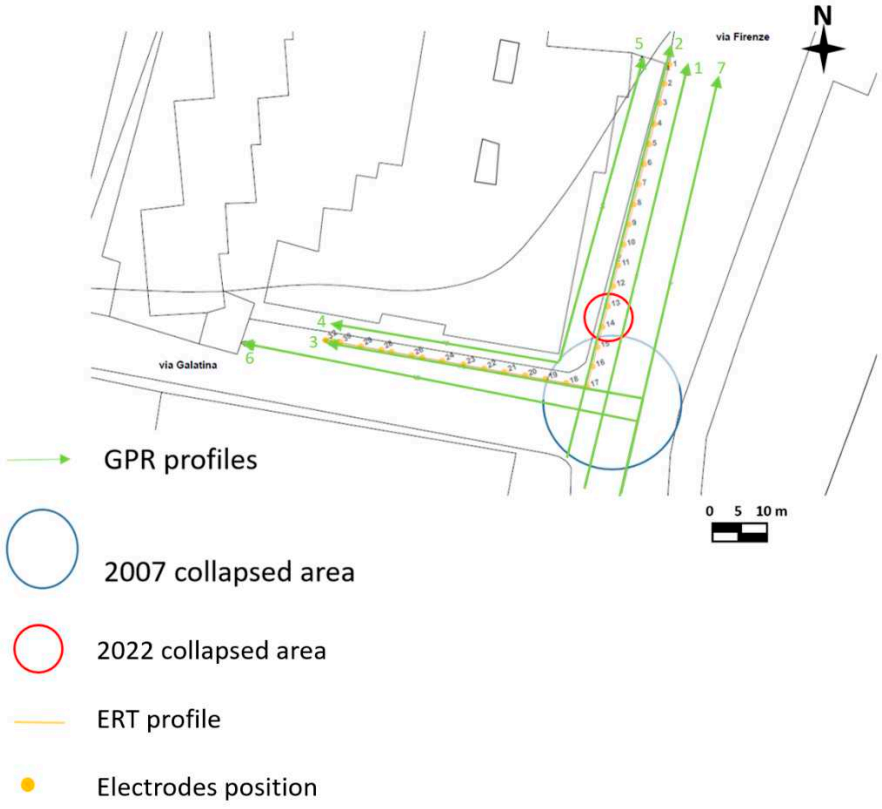

Figure 7. GPR and ERT surveyed areas in 2022.

For the second geophysical survey of 2022, ERT data were acquired using the MAE 600 E georesistivimeter with 32 active channels. In this case, the survey was performed using a particular geometry (L shape) to investigate below the building [13–16]. The L profile is shown in Figure 7. The dipole-dipole array was considered. It is the most used for cavities detection [13–16]. The distance between the electrodes was chosen equal to 1 m, and 32 electrodes were used. This type of array is well described in the international literature [14–16]. Initially, a 2D survey is conducted along each

Preprints (www.preprints.org) | NOT PEER-REVIEWED | Posted: 26 May 2023 doi:10.20944/preprints202305.1891.v1

perpendicular line or transect. In the next step, the current electrodes remain at the end of one line, while the potential is moved, along the line. Then, the current electrodes move one electrode position and the potential electrodes move as previously described. The process is repeated until the current and potential electrodes cover the L geometry. This sequence of observations produces a series of apparent resistivity observations towards and beneath the central portion of the array. The colored circles in Figure 8 represent the attribution points, where the apparent resistivities are measured, for the performed ERT array. This process is discussed in detail by [16].

Electrocardiogram electrodes were used to avoid piercing the floor [17–20]. Here the contact resistance was low (about 2000-3000 Ω m). This was probably due to the high humidity inside the church.

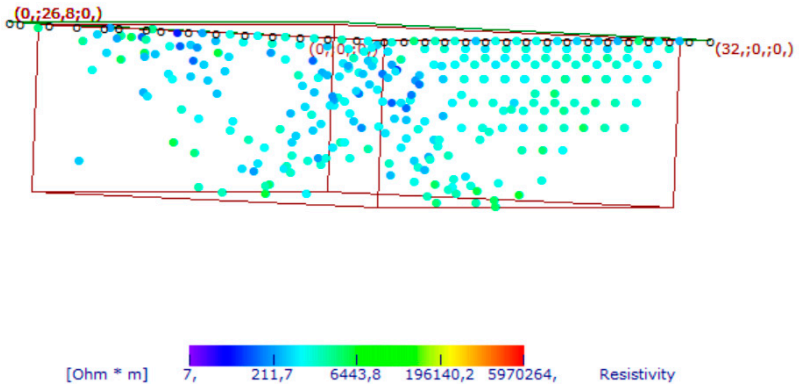

Figure 8. Apparent resistivity measured points. White circle represents the electrode location.

The ERTLab software (http://www.geostudiastier.it) was used to process the data in 3D mode. The software uses the tetrahedral finite element iterative method (data variance iterative reweighting).

3. Results

3.1. The 2007 GPR Data Analysis

3.1.1. Area A

In the area, A (Figure 5) were acquired, 17 parallel profiles 0.5 m spaced. The processed data (Figure 9) presents several reflection events. It presents a subsoil with backfill material for the first meter of depth. An interesting reflection event is denoted “C” in Figure 9a. It is evident in the first four profiles acquired in area A. The size is about 15 m wide and the depth of the top is between 2.6 and 3.2 m (with an average electromagnetic wave velocity of 0.108 m/ns).

Another interesting reflection event “C” (Figure 9b). The size is about 8 m wide, and the depth of the top, is between 2.4 and 2.8 m. Some considerations can be made to try to understand what C may be due to. Observing them on the radar sections, a change in the polarity of the electromagnetic wave (EM) is noted. An inversion of polarity is produced when the reflection coefficient is negative [10,11]. So, for materials where the wave velocity depends only on dielectric permittivity when radar waves are reflected in a material with a higher dielectric permittivity. A typical case is reflections from air to any other material [10,11]. All these considerations lead to interpreting these anomalies as being due to cavities.

Preprints (www.preprints.org) | NOT PEER-REVIEWED | Posted: 26 May 2023 doi:10.20944/preprints202305.1891.v1

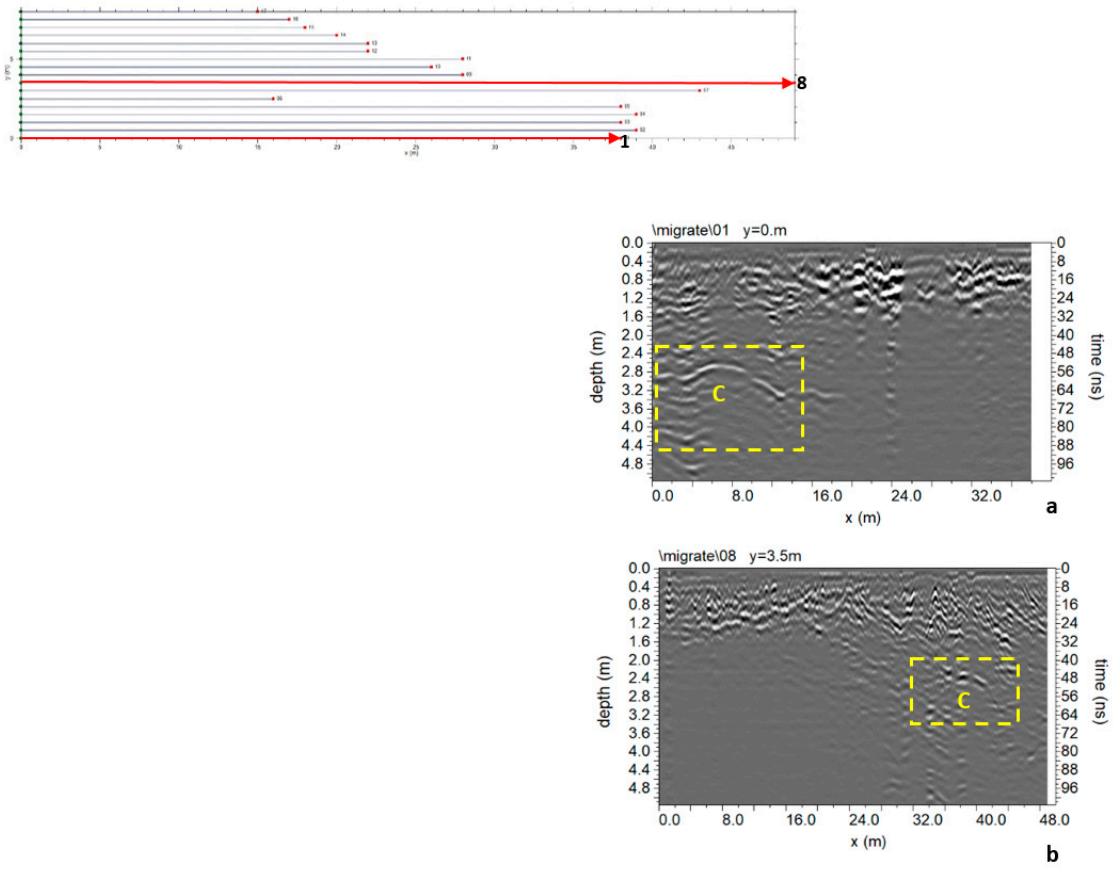

Figure 9. Area A: GPR processed data: a) profile n. 1; b) profile n. 8; C indicate a probable cavity.

A 3D map of the distribution of the anomalies identified within the 2D radar sections was built. One type of visualization is related to the construction of 2D time slices within specific time intervals [10,11]. In this work, time-slices have been built to visualize the amplitude variations within time intervals Δt = 10.4 ns. The overlay analysis was used [19–22].

Figure 10 shows the most significant time slices. Here the slices at depths between 2.1 m and 4.7 m are considered. In fact, at these depths, it is possible to highlight the reflected event linked to the C anomalies which correspond to the one indicated with C in the 2D radar section of Figure 9.

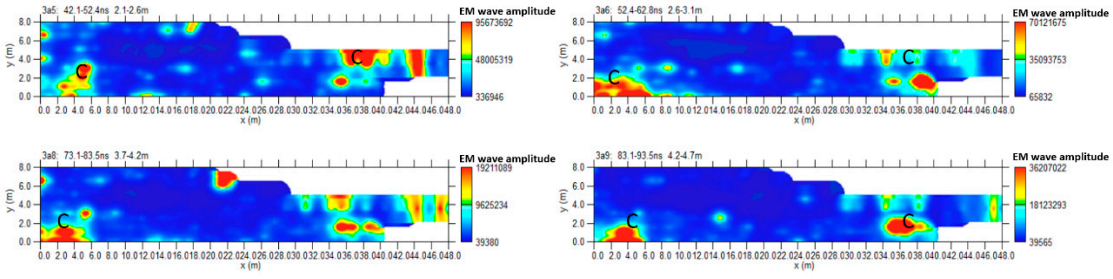

Figure 10. Area A: GPR time slices: C indicate a probable cavity.

Another way to present the 3D data volume is the amplitude iso-surfaces of the EM wave (Leucci, Conyers). Here it is possible to isolate the amplitude values; establishing a minimum threshold value in order to make make the 3D structure of the anomalies identified in the 2D radar sections uniquely visible. The threshold is a very delicate step and depends a lot on the experience of the interpreter to obtain valuable results [10,11].

Figure 11 shows the iso-surfaces amplitude with a threshold value equal to 65% of the total amplitude. Anomalies C can be visualized in their 3D development.

Preprints (www.preprints.org) | NOT PEER-REVIEWED | Posted: 26 May 2023 doi:10.20944/preprints202305.1891.v1

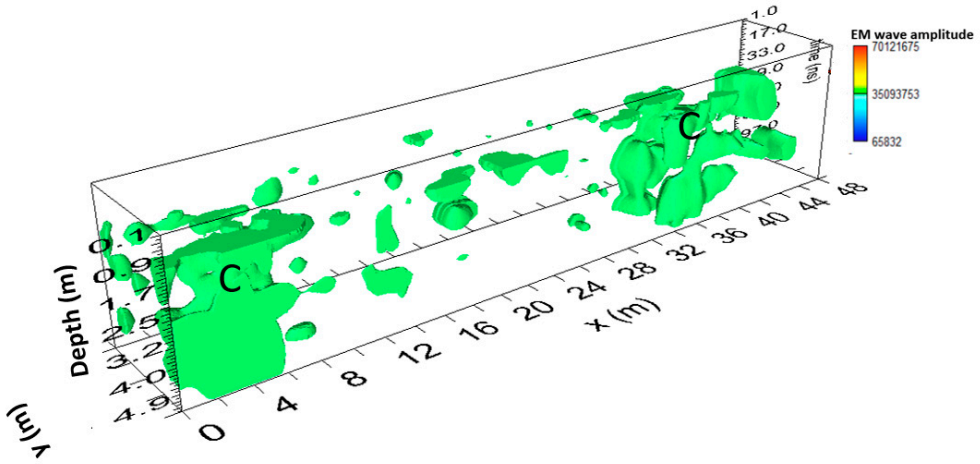

Figure 11. Area A: GPR iso-sufaces; C indicate a probable cavity.

3.1.2. Area B

In the area, B (Figure 5) were acquired 18 parallel profiles 0.5 m spaced. At the end of area B is the collapsed part of the road surface. Here the processed data shows an interesting reflection event "C" in Figure 12. It develops along the entire radar section at a depth between 2.0 m and 4.0 m. An inversion of polarity is noted and therefore this anomaly was probably due to cavities.

Figure 13 shows the most significant time slices. The slices at depths between 2.0 m and 3.1 m are considered. In fact, at these depths, it is possible to highlight the reflected event linked to the anomaly C.

Figure 14 shows the iso-surfaces amplitude with a threshold value equal to 70% of the total amplitude. Anomaly C can be visualized in its 3D development.

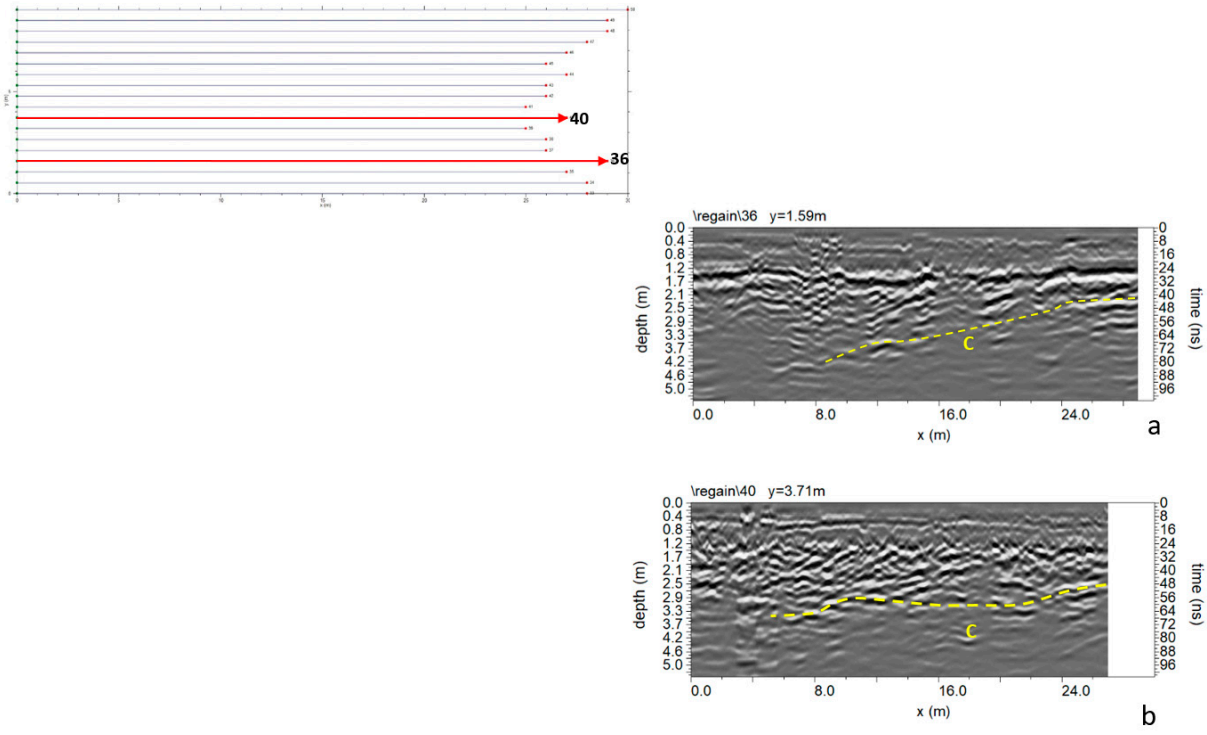

Figure 12. Area B: GPR processed data: a) profile n. 36; b) profile n. 40; C indicate a probable cavity.

Preprints (www.preprints.org) | NOT PEER-REVIEWED | Posted: 26 May 2023 doi:10.20944/preprints202305.1891.v1

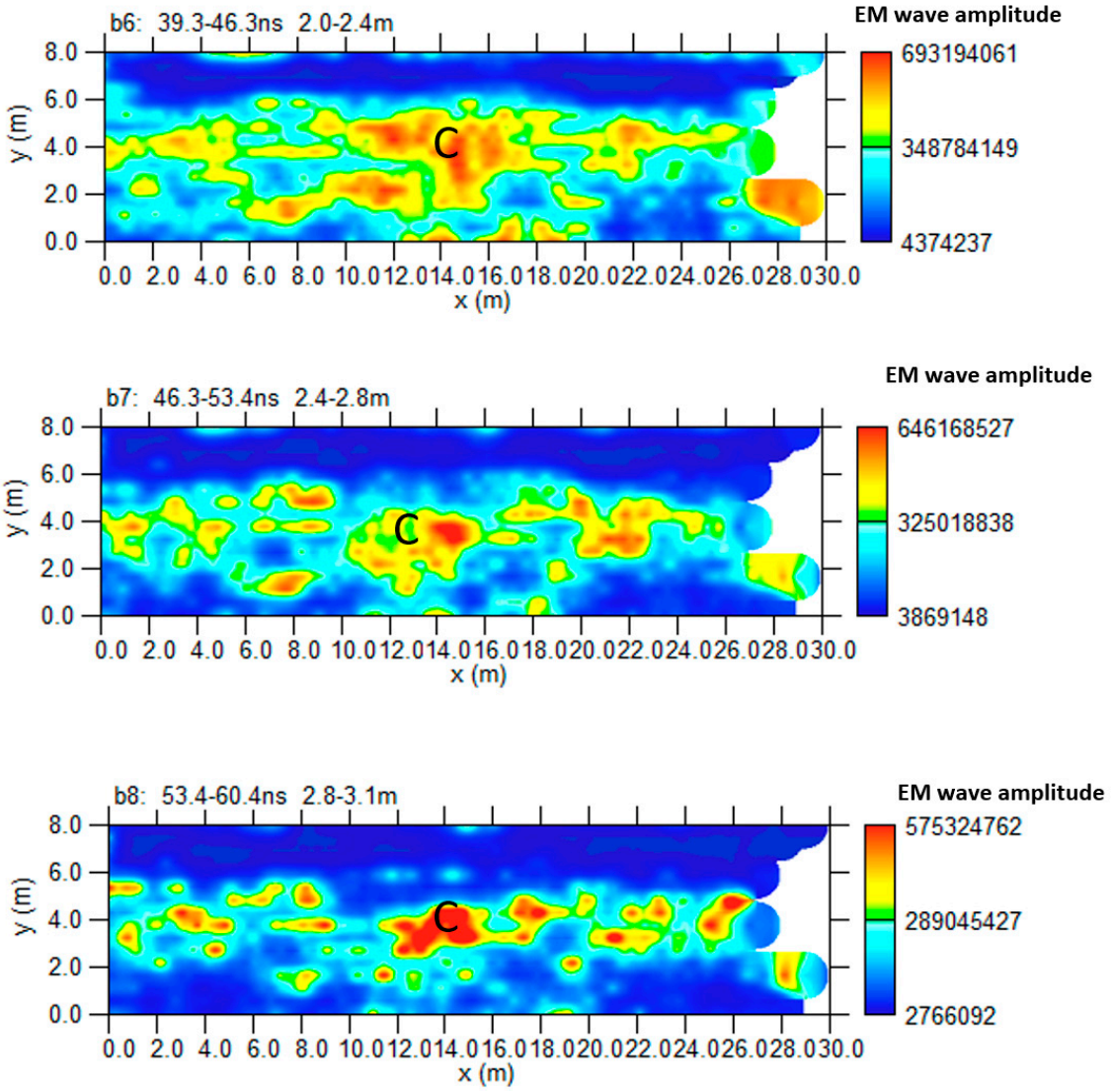

Figure 13. Area B: GPR time slices; C indicate a probable cavity.

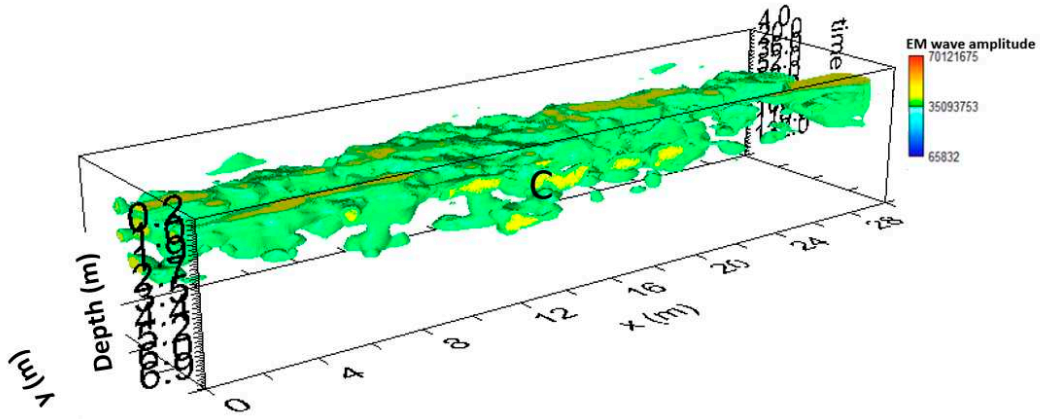

Figure 14. Area B: GPR iso-sufaces; C indicate a probable cavity.

3.1.3. Area C

Preprints (www.preprints.org) | NOT PEER-REVIEWED | Posted: 26 May 2023 doi:10.20944/preprints202305.1891.v1

In the area, C (Figure 5) were acquired 16 parallel profiles 0.5 m spaced. The GPR data analysis did not reveal any anomalies attributable to the presence of cavities (Figure 15).

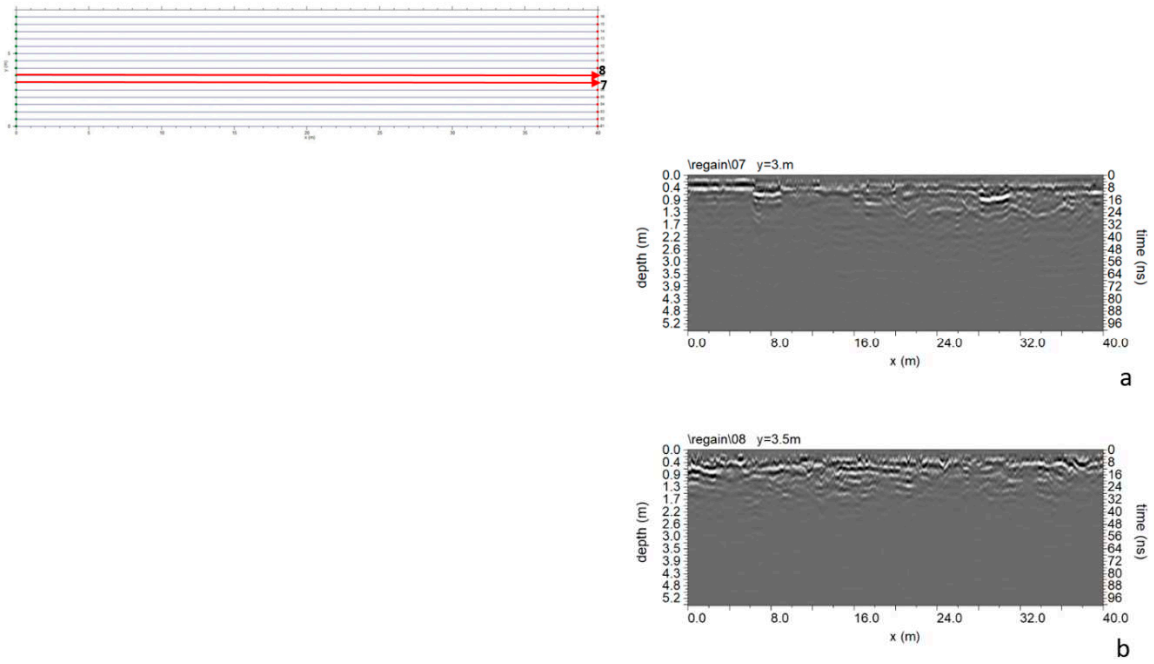

Figure 15. Area C: GPR processed data: a) profile n. 7; b) profile n. 8.

3.1.4. Area D

In the area, D (Figure 5) were acquired 8 parallel profiles 1.0 m spaced. The processed data shows an interesting reflection event "C" in Figure 16. It develops a depth between 1.6 m and 3.0 m. An inversion of polarity (Figure 17) is noted and therefore this anomaly was probably due to cavities.

Figure 18 shows the most significant time slices. The slices at depths between 1.1 m and 3.3 m are considered. In fact, at these depths, it is possible to highlight the reflected event linked to the anomaly C.

Figure 19 shows the iso-surfaces amplitude with a threshold value equal to 70% of the total amplitude. Anomaly C can be visualized in its 3D development.

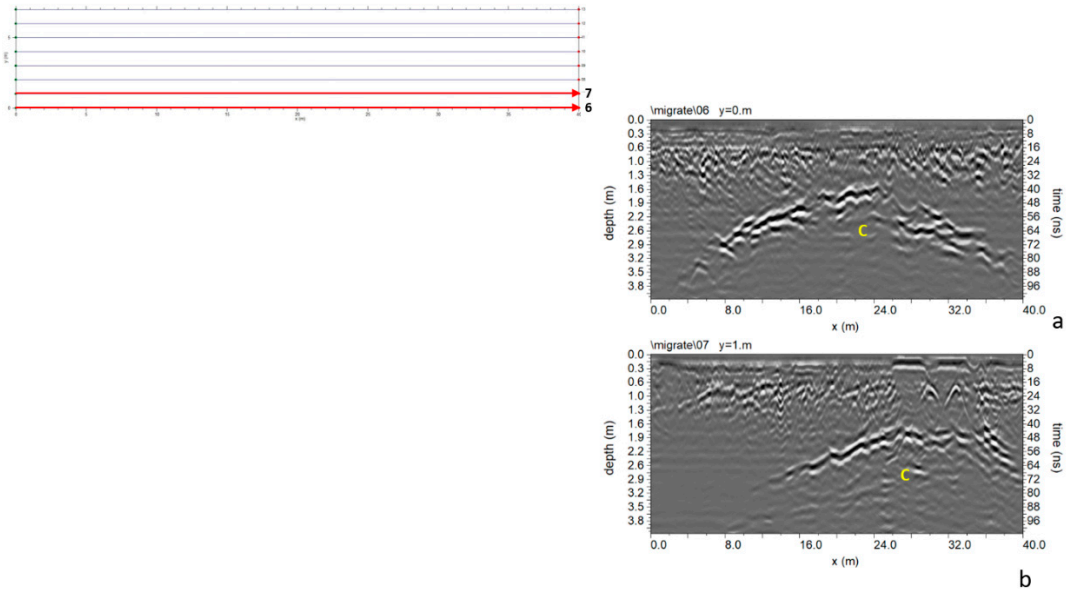

Preprints (www.preprints.org) | NOT PEER-REVIEWED | Posted: 26 May 2023 doi:10.20944/preprints202305.1891.v1

Figure 16. Area D: GPR processed data: a) profile n. 6; b) profile n. 7.

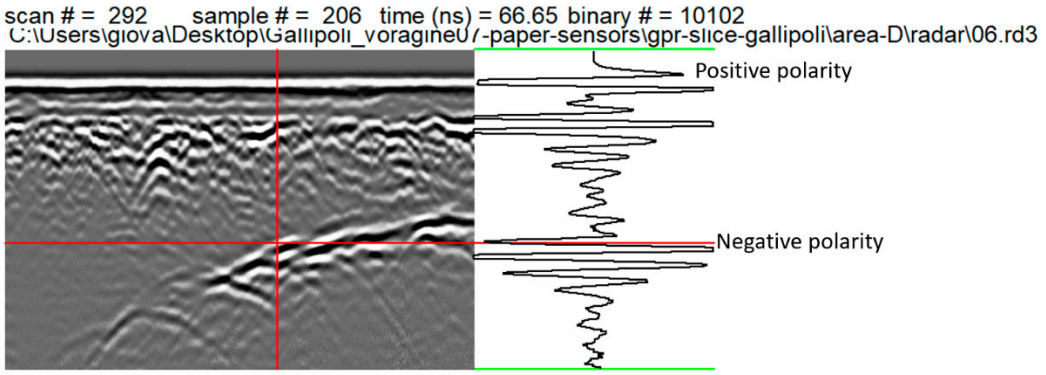

Figure 17. Area D: inversion of the polarity in the reflection event.

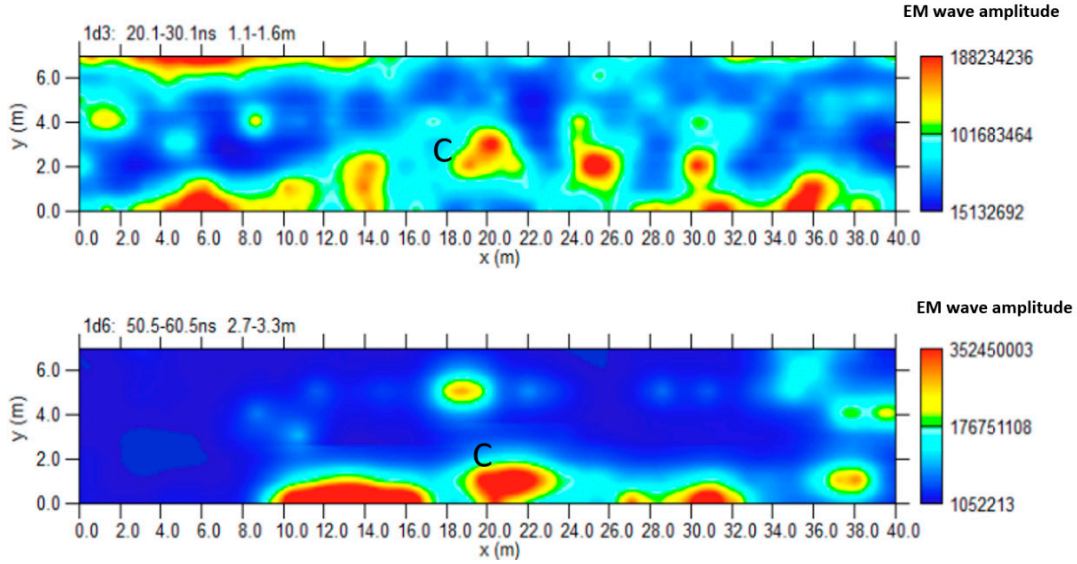

Figure 18. Area D: GPR Time slices; C indicate a probable cavity.

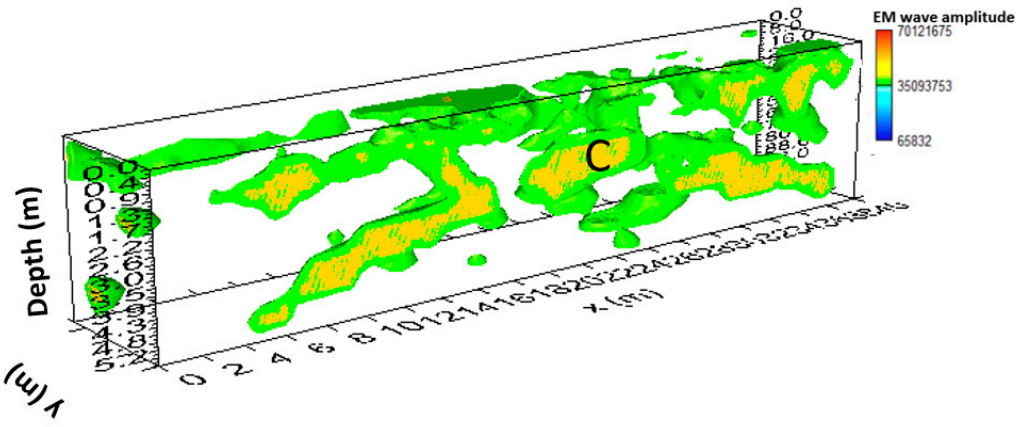

Figure 19. Area D: GPR iso-surfaces; C indicate a probable cavity.

Preprints (www.preprints.org) | NOT PEER-REVIEWED | Posted: 26 May 2023 doi:10.20944/preprints202305.1891.v1

3.1.5. Area E

In the area, E (Figure 5) were acquired 9 parallel profiles 0.85 m spaced. The processed data did not reveal any anomalies attributable to the presence of cavities (Figure 20).

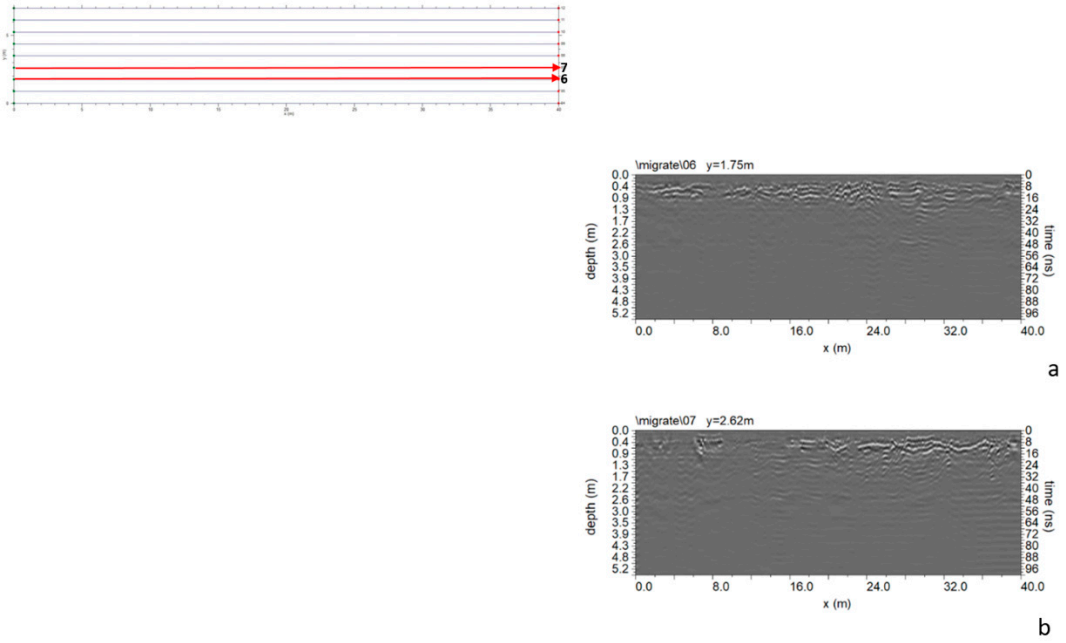

Figure 20. Area E: GPR processed data: a) profile n. 6; b) profile n. 7.

3.2. The 2022 GPR Data Analysis

The second subsidence event which occurred 15 years after the first made a second campaign of measures necessary. In this case some GPR profiles were performed to understand the extent of the phenomenon. Therefore the investigations were carried out only in the area affected by the second instability event. From the analysis of the data (Figure 21) it is possible to notice reflected events "C" which confirm the presence of the cavity. In fact here it is possible observe a polarity inversion of the reflected EM wave [10,11,20]

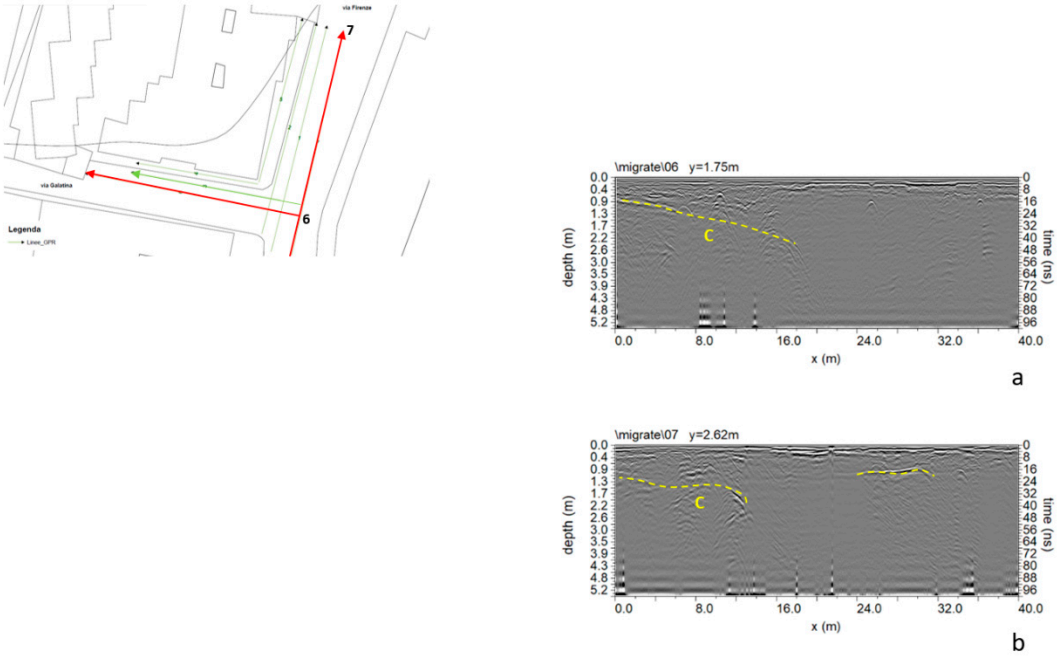

Preprints (www.preprints.org) | NOT PEER-REVIEWED | Posted: 26 May 2023 doi:10.20944/preprints202305.1891.v1

Figure 21. GPR processed data: a) profile n. 6; b) profile n. 7; C indicate a probable cavity.

3.3. The 2022 ERT Data Analysis

The ERT investigation was necessary to understand the possible development of the cavity underneath the buildings. For this reason, the acquisition geometry shown in Figure 7 was adopted. The 2D distribution of electrical resistivity as a function of the depth are shown in Figure 22.

From the 2D resistivity distribution (Figure 22) the presence of a heterogeneous subsoil with resistivity values between 2000 Ω m and 10000 Ω m is evident. In particular, is possible to note the presence of areas (indicated with C) with resistivity values between 2500 Ω m and 10000 Ω m which suggests the probable presence of cavities. These cavities seem to extend to a depth of about 4 m.

It is possible to build the ERT depth slices in order to visualize the distribution of the resistivity in a 3D mode below the investigated area within depth intervals. Here all the anomalies with the same resistivity values are interpolate and a 3D volume of resistivity data is built. Successively is possible to extract the 2D resistivity distribution at several depths. Figure 23 shows the most significant time slices.

From the analysis of the depth slices (Figure 23) is possible to see the distribution of the resistivity anomalies C below the investigated area.

Figure 24 shows the superimposition of the ERT results on the plan of the investigated area showing the position of probable cavity C.

Here it is possible to see how the cavity develops dangerously underneath the buildings.

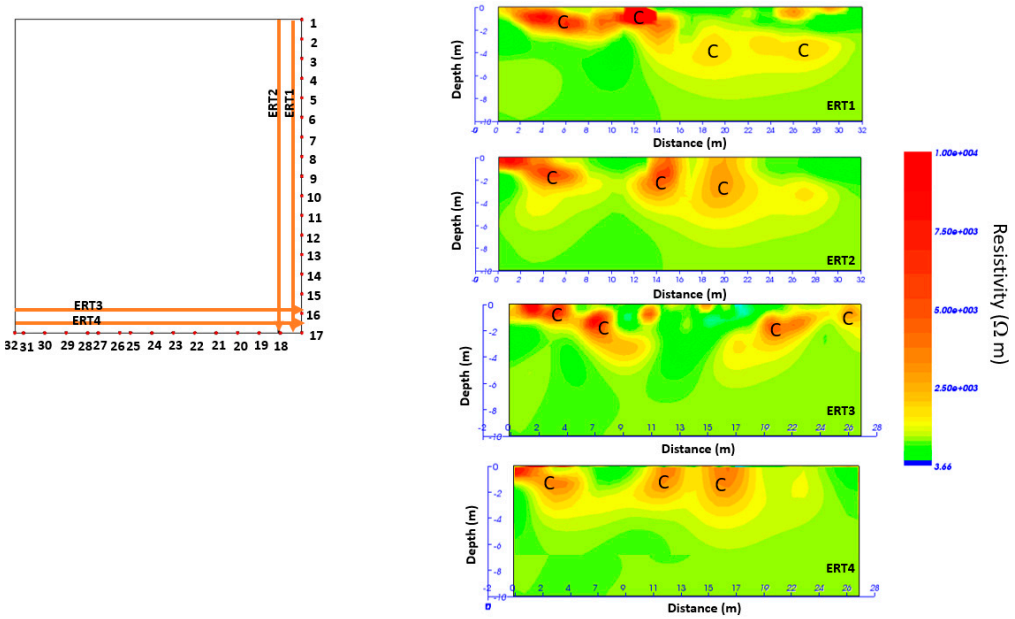

Figure 22. 2D resistivity distribution; C indicate a probable cavity.

Preprints (www.preprints.org) | NOT PEER-REVIEWED | Posted: 26 May 2023 doi:10.20944/preprints202305.1891.v1

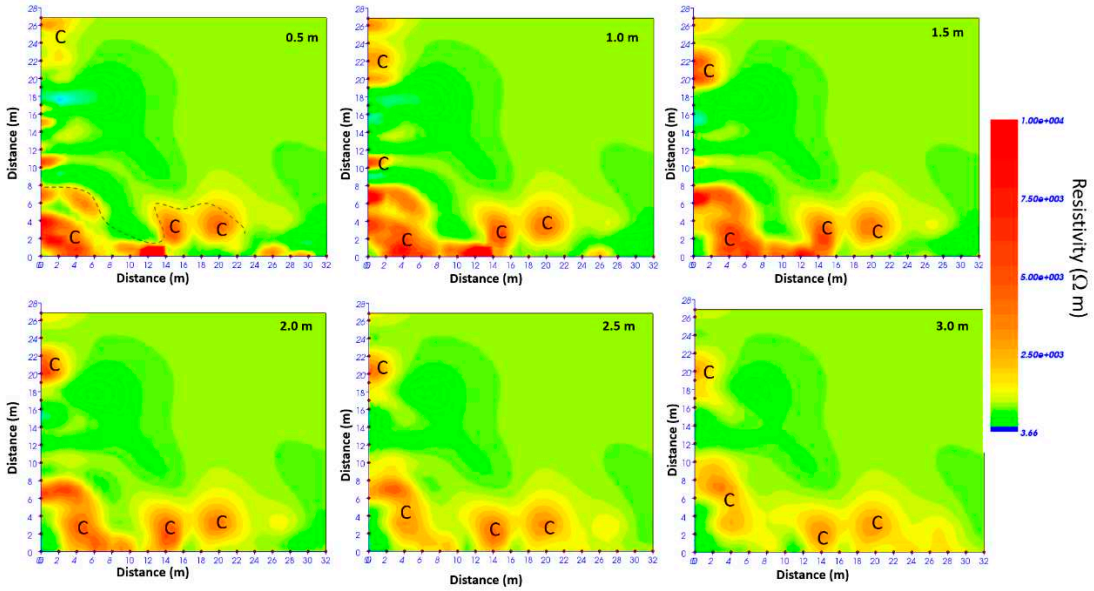

Figure 23. ERT depth slices; C indicate a probable cavity.

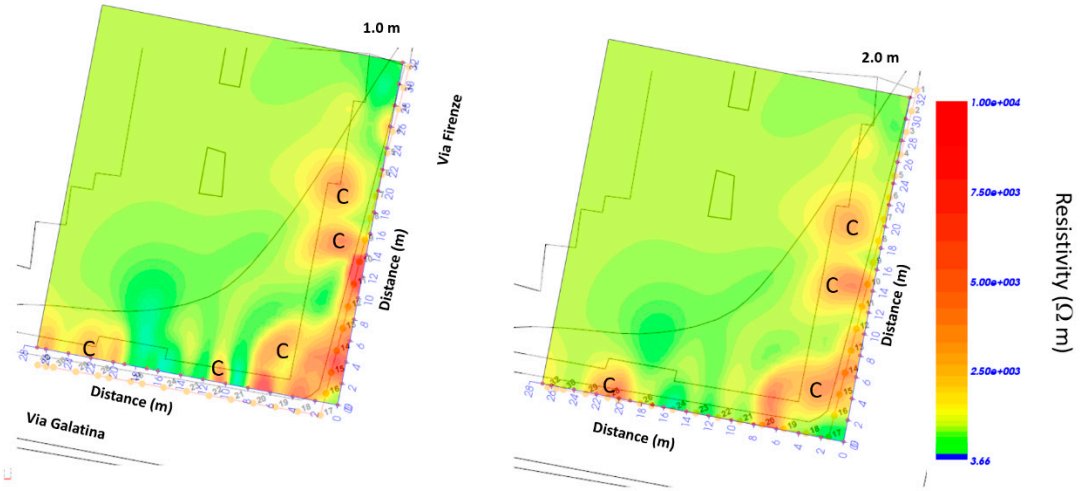

Figure 24. ERT depth slices overlapped to the planimetry; C indicate a probable cavity.

4. Discussion

Apart from the area affected by the collapse which was made safe, the geophysical investigation in the adjacent areas had the aim of understanding the stability conditions of the unexplorable cavities. The serious problem is found in areas where the roof thickness of the cavity was less than 5 m (areas A, B and D). In fact, as shown in Figures 7, 10 and 14, the thickness of the roof varies from 2.4 m (Figure 7), 2.9 m (Figure 9) to 1.9 m Figure 14. In this case, the buildings located near these areas could be in danger. Areas C and E were the most suitable for heavy vehicles to travel through for the first consolidation works. The area affected by the collapse was made safe with a consolidation intervention consisting of filling the cavities with concrete and strengthening of the pillars with the use of spritz - beton (shot concrete) inside which a filling of loose material (stone) was inserted. In Figure 25 the photos of the cavities after the intervention are shown.

In December 2022 (15 years after the first collapse event) another small collapse phenomenon occurred in the same area as the first collapse. There was a small hole with subsidence of the road pavement and cracks on the building (Figure 26a). The sagging of the pavement was also noticed inside the building (the photos are not shown for privacy reasons). For this reason, a geophysical

Preprints (www.preprints.org) | NOT PEER-REVIEWED | Posted: 26 May 2023 doi:10.20944/preprints202305.1891.v1

survey was decided to be limited to the area affected by the phenomenon. The GPR results show the presence of the cavity with a thinning of the roof thickness ranging from 0.9 m to 1.3 m (Figure 19). Very interesting are the ERT results that help us understand what happens underneath the building. Here we note the presence of cavities already at a depth of 0.5 m (Figures 20 and 21). The inspection of the cavity shows a probable deterioration of the consolidation intervention (Figure 26b)

Figure 25. Photos of the consolidation interventions.

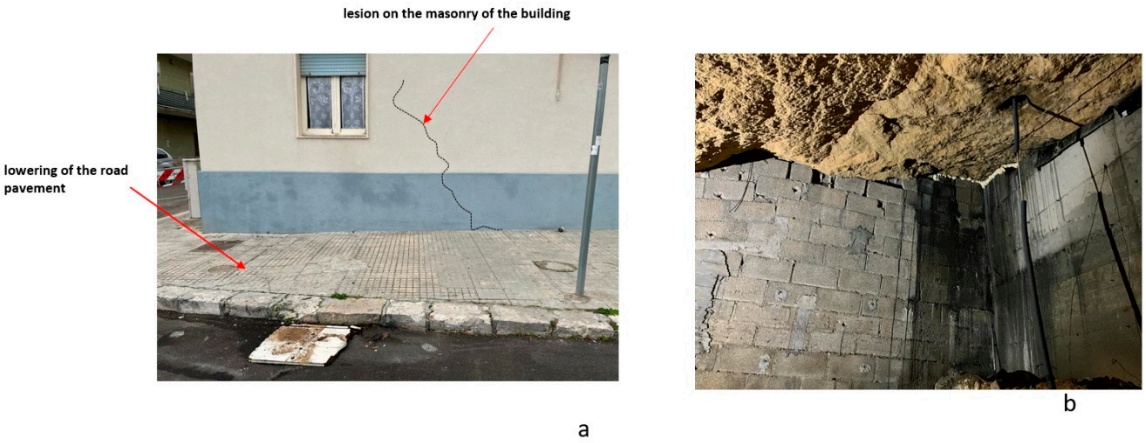

Figure 26. Photos: a) The December 2022 phenomenon; b) the cavity below the building after the consolidation interventions.

5. Conclusions

Immediately after the event at the end of March 2007, geophysical investigations became necessary to understand the development of the phenomenon and indicate the safest routes for rescuers to take for the first interventions. In this case, the geophysical survey using the GPR method showed the development of the cavity and the safest ways to go for the first interventions.

Subsequently, to make the cavity safe, a series of reinforced concrete pillars were built inside which a filling of loose material (stone) was inserted. Over the years this material (due to the abundant rains) has probably disintegrated causing the second instability event in December 2022. In this case, the integrated geophysical surveys ERT and GPR have highlighted the presence of voids where the fill had been made. Such voids are also present under the houses.

Author Contributions: Conceptualization, G.L.; methodology, L.D.G., D.F.B., C.T. and S.S..; software, L.D.G., D.F.B., C.T. and G.L.; validation, G.L.; formal analysis, L.D.G., D.F.B., C.T. and G.L.; investigation, S.S.; data curation, L.D.G., D.F.B., C.T., G.L. and S.S.; writing—original draft preparation, G.L.. All authors have read and agreed to the published version of the manuscript

Funding: Please add: "This research received no external funding".

Institutional Review Board Statement: Not applicable

Informed Consent Statement: Not applicable

Data Availability Statement: The data presented in this study are available on request from the corresponding author

Conflicts of Interest: The authors declare no conflict of interest

References

1. Corazza, A. Censimento dei dissesti dovuti a cavità sotterranee in Italia. *Atti del convegno Stato dell'arte sullo studio dei fenomeni di sinkholes e ruolo delle amministrazioni statali e locali nel governo del territorio* **2004**, *233-244*.
2. Delle Rose M. Mediterranean Pliocene events in the salento geological records. Thalassia Salentina, **2006,** 29, 77-99
3. Delle Rose M. and Federico A.. Karstik phenomena and environmental hazard in salento coastal plains.Proceedings IX IAEG Congress Engineering Geology for developing countries. **2002**, 1297-1305.
4. Leucci G. and De Giorgi L. Microgravimetric and ground penetrating radar geophysical methods to map the shallow karstic cavities network in a coastal area (marina di capilungo, lecce –italy). *Exploration Geophysics*, **2010**, 41, 178-188;
5. Leucci, G, Contribution of ground-penetrating radar and electrical resistivity tomography to identify the cavity and fractures under the main church in botrugno (Lecce, Italy). *Journal of Archaeological Science*, **2006**, 33, 1194-1204
6. Van schoor, M. Detection of sinkholes using 2D electrical resistivity imaging: *Journal of Applied Geophysics*, 2002, 50, 393–399,
7. Lai, W. W. L., Chang R. K. W., and Sham J. F. C. A blind test of nondestructive underground void detection by ground penetrating radar (GPR). *Journal of Applied Geophysics*, **2018**,
8. Tao M. , Chen X., Cheng Q., and Binley A. Evaluating the joint use of GPR and ERT on mapping shallow subsurface features of karst critical zone in southwest China. *Vadose Zone Journal*, **2021**, DOI: 10.1002/vzj2.20172
9. Conyers L.B.. Ground-penetrating Radar for Archaeology. *Altamira Press*, 2004, Walnut Creek, California.
10. Conyers L.B. Innovative ground-penetrating radar methods for archaeological mapping. *Archaeological Prospection*, **2006**, 13(2): 139–141.
11. Conyers L.B. Interpreting Ground-penetrating Radar for Archaeology. *Left Coast Press*, **2012**, Walnut Creek, CA.
12. Joshi, Mayank, P. R. Prasobh, S. Rajappan, B. Padma Rao, Alka Gond, Anshuman Misra, K. Eldhose, V. Nandakumar, and J. K. Tomson. "Detection of soil pipes through remote sensing and electrical resistivity method: Insight from southern Western Ghats, India." Quaternary International 575 (2021): 51-61.
13. Hussain Y., Uagoda R., Borges W., Nunes J., Hamza O., Condori C., Aslam K., Dou J., and Cárdenas-Soto M. The Potential Use of Geophysical Methods to Identify Cavities, Sinkholes and Pathways for Water Infiltration. *Water* **2020**, 12, 2289; doi:10.3390/w12082289.
14. Argote-Espino D, Tejero-Andrade A, Cifuentes-Nava G, Iriarte L, Farıas S, Chavez RE, Lopez F (2013) 3D electrical prospection in the archaeological site El Pahnu, Hidalgo State, Central Mexico. J Archaeol Sci 40:1213–1223
15. Chavez G, Tejero A, Alcantara MA, Chavez RE (2011) The 'L-Array', a tool to characterize a fracture pattern in an urban zone: in expanded abstracts: near surface 2011. Eur As Geosci Eng 1:114–155
16. Tejero-Andrade A, Cifuentes G, Chavez RE, Lopez Gonzalez A, Delgado-Solorzano C (2015) ''L'' and ''Corner'' arrays for 3D electrical resistivity tomography: an alternative for urban zones. Near Surf Geophys 13:1–13. doi:10.3997/1873-0604.2015015

17. Arisona A., Ishola K. S. and Nawawi M. N. M. Subsurface void mapping using geophysical and geotechnical techniques with uncertainties estimation: case study of Kinta Valley, Perak, Malaysia *SN Applied Sciences*, **2020,** 2:1171 | https://doi.org/10.1007/s42452-020-2967-x
18. Amanatidou E., Vargemezis G., and Tsourlos P. Combined application of seismic and electrical geophysical methods for karst cavities detection: A case study at the campus of the new University of Western Macedonia, Kozani, Greece. Journal of Applied Geophysics **2022**, Volume 196, January 2022, 104499
19. Leucci G. Nondestructive Testing for Archaeology and Cultural Heritage: A practical guide and new perspective. *Springer* **2019**, pp 217, ISBN 978-3-030-01898-6
20. Leucci G. Advances in Geophysical Methods Applied to Forensic Investigations: New Developments in Acquisition and Data Analysis Methodologies. *Springer* **2020**,pp 200, ISBN 978-3-030-46241-3
21. Goodman D, Piro S. GPR Remote Sensing in Archaeology. *Geotechnologies and the Environment Series*, . **2013**, Vol. 9, Springer-Verlag: Berlin; 233 pp.
22. Goodman D, Steinberg J, Damiata B, Nishimure Y, Schneider K, Hiromichi H, Hisashi N. *GPR overlay analysis for archaeological prospection*. Proceedings of the 11th International Conference on Ground Penetrating Radar, Columbus, Ohio, 2006, CD-rom